WILEY | Hindawi

Research Article

Research on Crack Propagation of Deep Geologic Mass Disturbed by Excavation Based on Phase Field Method

Ningdong Chang [ID],[1] **Jinan Wang** [ID],[1,2] **and Fei Li** [ID][1]

[1]*School of Civil and Resource Engineering, University of Science and Technology Beijing, Beijing 100083, China*
[2]*Key Laboratory of Ministry of Education for Efficient Mining and Safety of Metal Mines, Beijing 100083, China*

Correspondence should be addressed to Fei Li; lifei2016@ustb.edu.cn

In recent years, the phase field fracture model has been widely studied and applied. It has good convergence in crack propagation simulation. Comparing with other methods, the phase field method has advantages in simulating crack intersection, bifurcation, and three-dimensional propagation. Based on the phase field method, the influence of excavation disturbance on crack initiation of rock mass is realized in this paper. The phase field fracture variational model is built by using user-defined element interface (UEL) and user material subroutine (UMAT) in ABAQUS. Firstly, the prefabricated crack propagation simulation is carried out to verify the algorithm. The fracture initiates in a butterfly shape and then expands along the horizontal direction. The results show that the maximum support reaction decreases with the gradual increase of l, which is compared with the results obtained by Miehe et al. The result proved the correctness and reliability of the algorithm. In this paper, the phase field fracture model of a flat plate with a reserved small hole under the upper tension is established. The results show that the crack finally produces a crack in the lower left and upper right directions of the square hole and continues to extend to the model boundary, which proves the feasibility of crack independent initiation and propagation by the phase field method. The stress formed a butterfly region until the fracture occurs. And the butterfly stress distribution was still present at the end of crack propagation. The maximum vertical stress was 1.7×10^3 MPa. Based on the South-to-North Water Transfer Project, the simulation of tunnel crack propagation under excavation disturbance is realized for the first time, which is based on the phase field method. The results show that the influence area of excavation disturbance will increase after considering crack development. Comparing the simulation results without considering crack propagation with the simulation results considering crack propagation, it is found that the stress level in the excavation disturbance area around the tunnel is greatly affected by cracks. When the crack is not considered, the maximum vertical stress is 2.16×10^5 Pa, and the maximum horizontal stress is 9.35×10^5 Pa, which occurs at the waist of the tunnel on the horizontal axis. When the crack is considered, the maximum vertical stress is 2.53×10^5 Pa, and the maximum horizontal stress is 1.10×10^6 Pa. It shows that the stress at the dome increases greatly. The vertical stress reaches 3.68×10^5 Pa, and the horizontal stress is up to 3.07×10^3 Pa. For the rock mass far away from the excavation disturbance area, because part of the elastic strain energy is absorbed by the surface crack, the stress level considering the crack is lower than that without the crack. But it is basically similar, indicating the accuracy of the phase field fracture model. This paper realizes the simulation of crack propagation under excavation disturbance and provides a way for the application of phase field fracture model in rock mechanics. This paper proves that phase field method has broad prospects in simulating rock crack propagation and provides the possibility for the popularization of phase field method.

1. Introduction

In rock engineering, crack initiation and development are the main failure modes of rock. The crack development eventually leads to rock fracture [1, 2]. The crack develop-ment also leads to local stress disturbance. Therefore, numerical simulation of fracture is of great significance in the field of geotechnical engineering.

At present, finite element methods for crack propagation can be divided into two categories: One is geometric crack
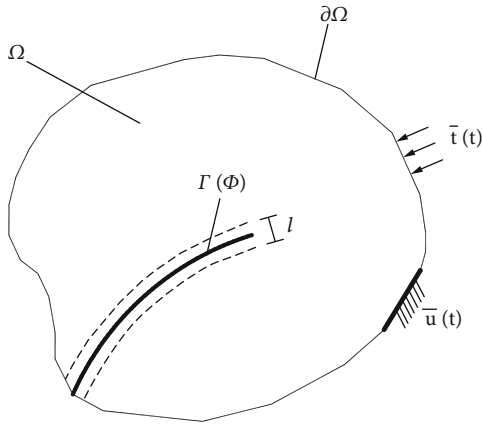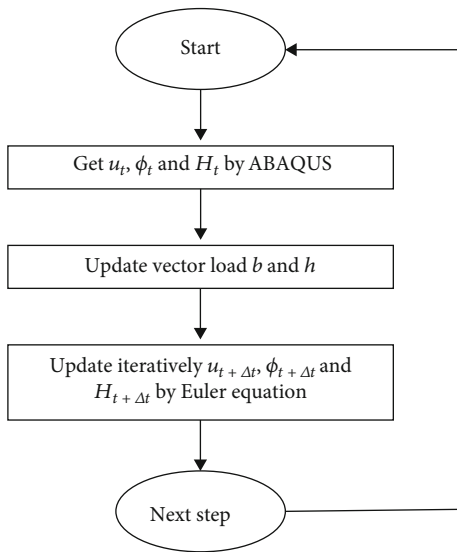
FIGURE 1: Crack described with a phase field mode.
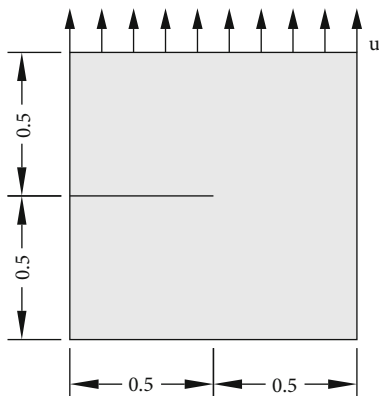

FIGURE 2: The process for solving phase field model.

FIGURE 3: Geometric model and the location of crack (mm).

the fracture critical [4]. The interface element method [5, 6] inserts cohesive interface elements between elements. When reached the critical condition of fracture, the interface element will be disconnected. The interface element method only allows the crack to expand on the boundary of the element [7]. This type of approach allows Raven to extend only at the boundaries of the cell. The other is the nongeometric description method, which is the diffusion crack model, such as the smooth particle hydrodynamics (SPH), the diffuse element method (DFM), the extended finite element method (XFEM), and phase field methods. Lucy and Gingold first applied the smooth particle hydrodynamics in the field of astrophysics [8, 9]. Nayrole et al. proposed the scatterer method in 1992 [10]. This method is collectively known as the meshless method. Although the meshless method does not need element structure, its crack propagation needs manual setting, and its computational efficiency is very low. Extended finite element method (XFEM) [11, 12] combined displacement field related parameters with variational function and test function by using the shape function. The fracture has nothing to do with the grid by using XFEM. The expansion of cracks can be achieved within the grid, but its calculation is limited to a few relatively simple bifurcation problems of crack. It is difficult to solve the three-dimensional model of crack propagation simulation [13, 14]. The phase field method [15] used the dispersed phase boundary to approximate the actual sharp boundary, which implemented a model describing fracture with continuous functions. By using phase field variables, the phase field method can explicitly track crack, instead of tracking the surface of crack. The propagation path of crack can be obtained by the evolution of order parameters. So, the phase field method of crack propagation simulation is not affected by meshing. Moreover, it has good convergence [16] and can also realize crack propagation in the grid.

In recent years, phase field model has been applied to fracture field. It has attracted extensive attention in this field. Emilio [17] realized the operation of phase field fracture model in user-defined unit interface (UEL) and user material subroutine (UMAT) of ABAQUS, but the model is simple. Hofacker [18, 19] established the evolution of complex crack mode for dynamic problems and applied interlacing algorithm to phase field simulation. He provided the basis for solving dynamic problems. Park [20] realized the refinement model of adaptive grid and carried out the simulation of cohesive cracks under dynamic loading. Liu Guowei [21] used ABAQUS platform to realize the step algorithm of phase field fracture model and analyzed the problem of two parallel air foil crack intersection. Cao Yakuo [22] studied the fracture process of elastic-plastic plate with holes at different spatial distances based on the elastic-plastic fracture theory of metal. It provided a thought for solving the elastic-plastic problem. Liu Jia [23] established a phase field model of hydraulic coupling based on porous elasticity theory and energy minimization theory. It solves the problem of phase field seepage.

The phase field fracture method describes the physical process of fracture through a series of differential equations, so as to avoid the tedious crack surface tracking. It has great advantages in simulating crack initiation, propagation, and

description method based on grid expansion, such as element deletion method [3] and interface element method. The element deletion method is a relatively simple method to describe the crack by discontinuous means. In this method, the stress of the element becomes 0 when it reaches

(a)

(b)

(c)
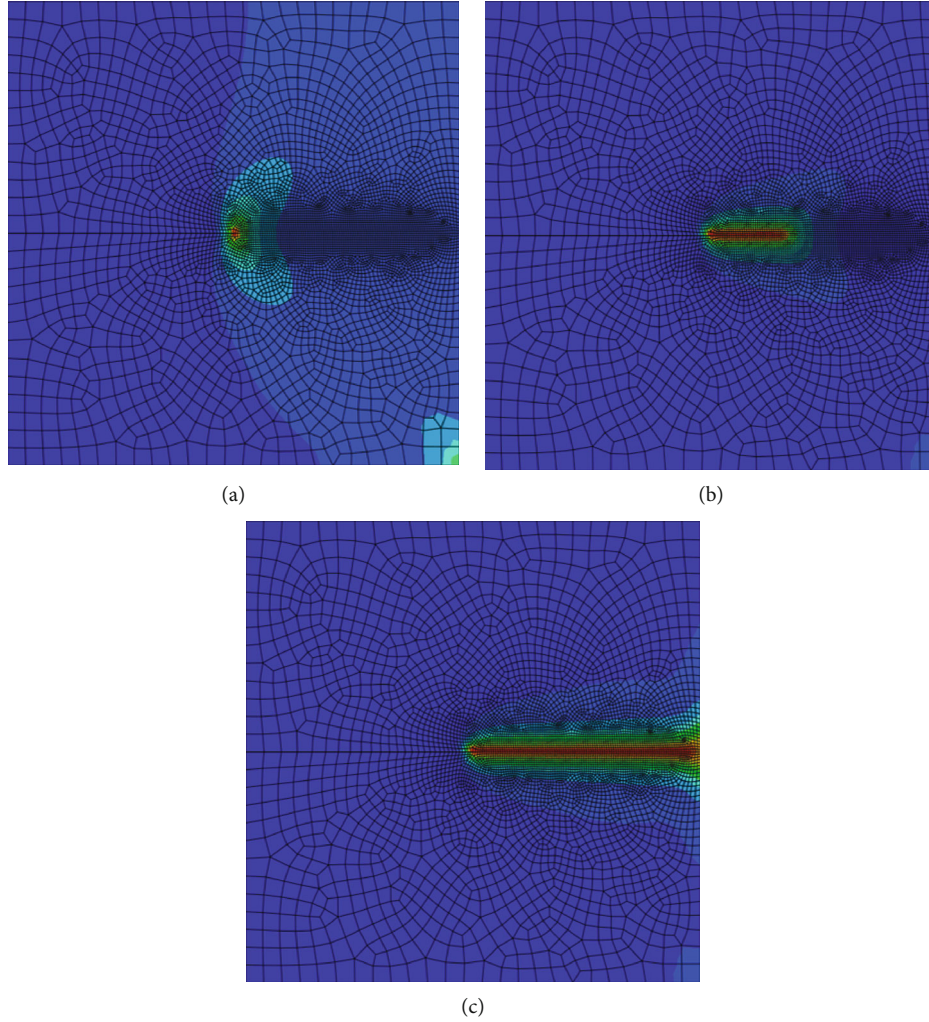
Figure 4: The propagation of crack when $l = 0.015$mm. (a) Crack initiation stage. (b) Crack development stage. (c) Crack penetration stage.

bifurcation. At present, most of the phase field method simulation is a two-dimensional simple model of single homogeneous material, and there is no correlation analysis of excavation disturbance. Based on the phase field method, this paper established a composite stratum model and realized the excavation simulation by element deletion.

In this paper, the user-defined element (UEL) of finite element software ABAQUS is used to calculate the propagation of prefabricated crack and the crack propagation of perforated plate during tensile, which verified the correctness of the code. The deep rock mass disturbed by excavation will crack on the excavation boundary, which will lead to local stress concentration of rock mass. Finally, rock mass will break and be instability. Therefore, it is of great significance to study the stress distribution of deep rock mass disturbed by excavation.

2. Phase Field Method Fracture Model

2.1. Fracture Variational Theory. The phase field method is based on Ginzburg-Laudau theory. Hakim and Karma proposed the phase field model [15], which defines the free energy of the fracture system as follows:

$$F(u, s) = \int \left\{ g(\phi)[\psi_0(\varepsilon(u)) - \psi_c] + V(\phi) + \frac{1}{2}D_\phi|\nabla\phi|^2 \right\} dx,$$

$$(1)$$

where ϕ is the order parameter; $g(\phi)$ is the interpolation function, $g(\phi) = \phi^{2+\alpha}$; ψ_0 is strain energy density; ψ_c is the critical strain energy density; $V(\phi)$ is the two potential well function, $V(\phi) = \phi^2(1-\phi^2)/4$; and D_ϕ is surface parameter. The first two terms are the body free energy term and the last term is the surface energy term.

In 1920, Griffith proposed Griffith energy theory based on energy [24], but this theory is suitable for simple model. It is difficult to analyze the complex crack model. In 1998, G. A. Francfor and J. J. Marigo proposed a variational method for fracture problems, which was based on the Griffith energy theory [25]. The total potential energy Π of elastomer Π can be divided into elastic energy of elastomer and
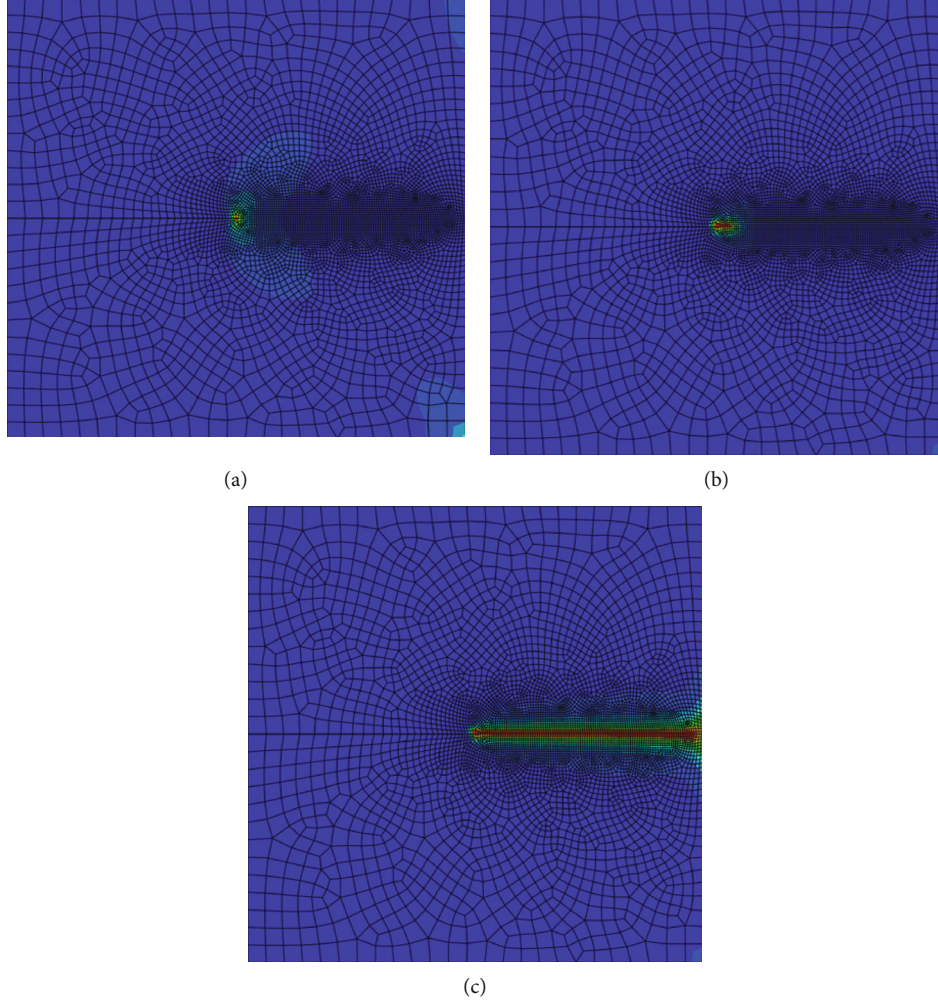
(a)

(b)

(c)

FIGURE 5: The propagation of crack when $l = 0.0075$mm. (a) Crack initiation stage. (b) Crack development stage. (c) Crack penetration stage.

surface energy of fracture:

$$\prod(u, \Gamma) = \int_{\Omega} \psi_e(\varepsilon(u))d\Omega + \int_{\Gamma} G_c d\Gamma, \tag{2}$$

where ψ_e is the elastic energy density; $\varepsilon(u)$ is the strain tensor; and G_c is the critical energy release rate.

In the fracture variational model proposed by Francfor and Marigo, the crack propagation is controlled by the principle of minimum free energy. However, the boundary integral of surface energy in this method is not easy to deal with in the case of unknown crack boundary. In 2000, Bourdin and Francfort introduced the order parameter [26] and defined one in the interval [0, 1]. When $\phi = 0$, it means that the material is intact. When $\phi = 1$, it means that the material is completely fractured, as shown in Figure 1. The crack surface density can be expressed as

$$\gamma(\phi, \nabla\phi) = \frac{1}{2l}\phi^2 + \frac{l}{2}|\nabla\phi|^2, \tag{3}$$

where l is the characteristic length parameter and the time length parameter determines the diffusion degree of the

crack. When $l \longrightarrow 0$, the characterization is closer to the tip crack. However, the size of L does not represent the actual width of crack diffusion.

Then, the total surface energy of cracks in the elastic body can be expressed as

$$\int_{\Gamma} G_c d\Gamma \approx \int_{\Omega} G_c \left[\frac{(\phi - 1)^2}{2l} + \frac{l}{2}|\nabla\phi|^2 \right] d\Omega, \tag{4}$$

where G_c is the critical value of Griffith energy release rate of material per unit area.

To analyze the fracture phase field, the total energy function of the material can be expressed as

$$\Psi(u, \phi) = \Psi^b(u, \phi) + \Psi^s(\phi), \tag{5}$$

where $\Psi^b(u, \phi)$ is the elastic strain energy stored in the material and $\Psi^s(\phi)$ is the surface strain energy related to the crack.
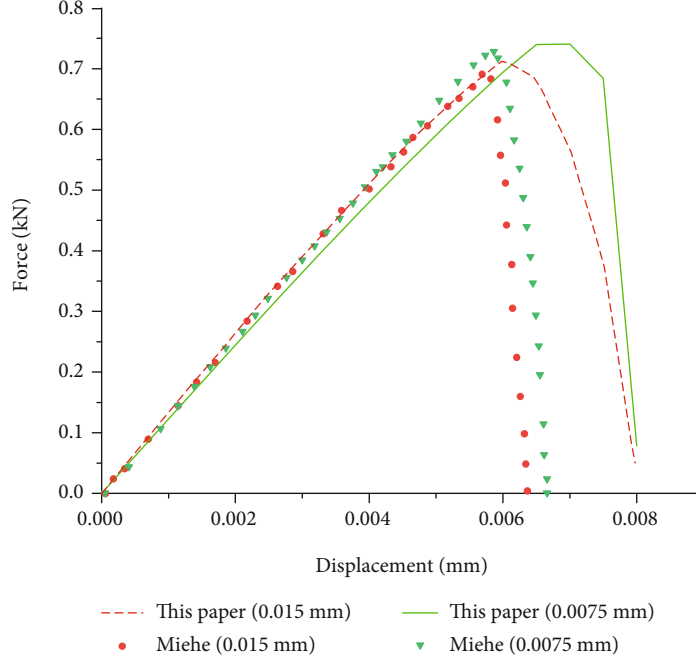
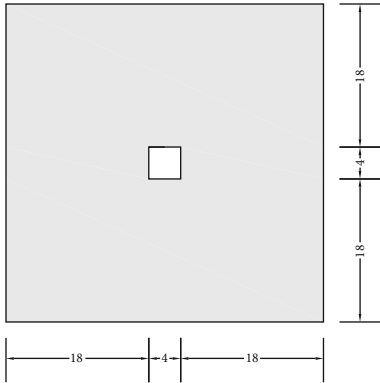FIGURE 6: Comparison of load-displacement curves of different l.

FIGURE 7: Prefabricated cavity plate model (m).

The elastic strain energy can be expressed by the elastic strain as

$$\Psi^b(u, \phi) = \int_\Omega \psi(\varepsilon(u), \phi)dV, \quad (6)$$

where u is the displacement of material; ϕ is the fracture phase field variable; energy storage function ψ of material per unit volume can be expressed as $\psi(\varepsilon, \phi) = g(\phi)\psi_0(\varepsilon)$; ψ_0 is the elastic strain energy density; $g(\phi)$ can be expressed as $g(\phi) = (1 - \phi)^2 + k$, and k is a very small constant.

Based on the above formula, the total energy function of materials can be expressed as

$$\Psi(u, \phi) = \int_\Omega \left\{ \left[(1 - \phi)^2 + k\right]\psi_0(\varepsilon) + G_c \left[\frac{1}{2l}\phi^2 + \frac{l}{2}|\nabla\phi|^2\right] \right\}dV, \quad (7)$$

2.2. Fracture Governing Equation by Phase Field Method. The energy of the system can be divided into external work generated by the application of load and internal work generated by deformation. The external energy increment δW_{ext} can be expressed as

$$\delta W_{\text{ext}} = \int_V b\delta u dV + \int_{\delta V} h\delta u\partial V, \quad (8)$$

where b is the body force per unit volume unit and h is the boundary surface force per unit area.

The change of internal potential energy increment is

$$\partial W_{\text{int}} = \partial \psi = \frac{\partial \psi}{\partial \varepsilon}\delta\varepsilon + \frac{\partial \psi}{\partial \phi}\delta\phi. \quad (9)$$

Combined with Equation (7), the internal potential energy increment can be expressed as

$$\partial W_{\text{int}} = \int_\Omega \left\{ \sigma\delta\varepsilon - 2(1 - \phi)\delta\phi\psi(\varepsilon) + G_c \left[\frac{1}{l}\phi\delta\phi + l\nabla\phi \cdot \nabla\delta\phi\right] \right\}dV, \quad (10)$$

where σ is Cauchy stress tensor,

$$\sigma = \frac{\partial \psi}{\partial \varepsilon} = g(\phi)\sigma_0 = \left[(1 - \phi)^2 + k\right]\sigma_0. \quad (11)$$

Assuming that the model is a quasi-static process, the virtual work done by the external force of the structure is equal to the virtual work done by the internal force of the
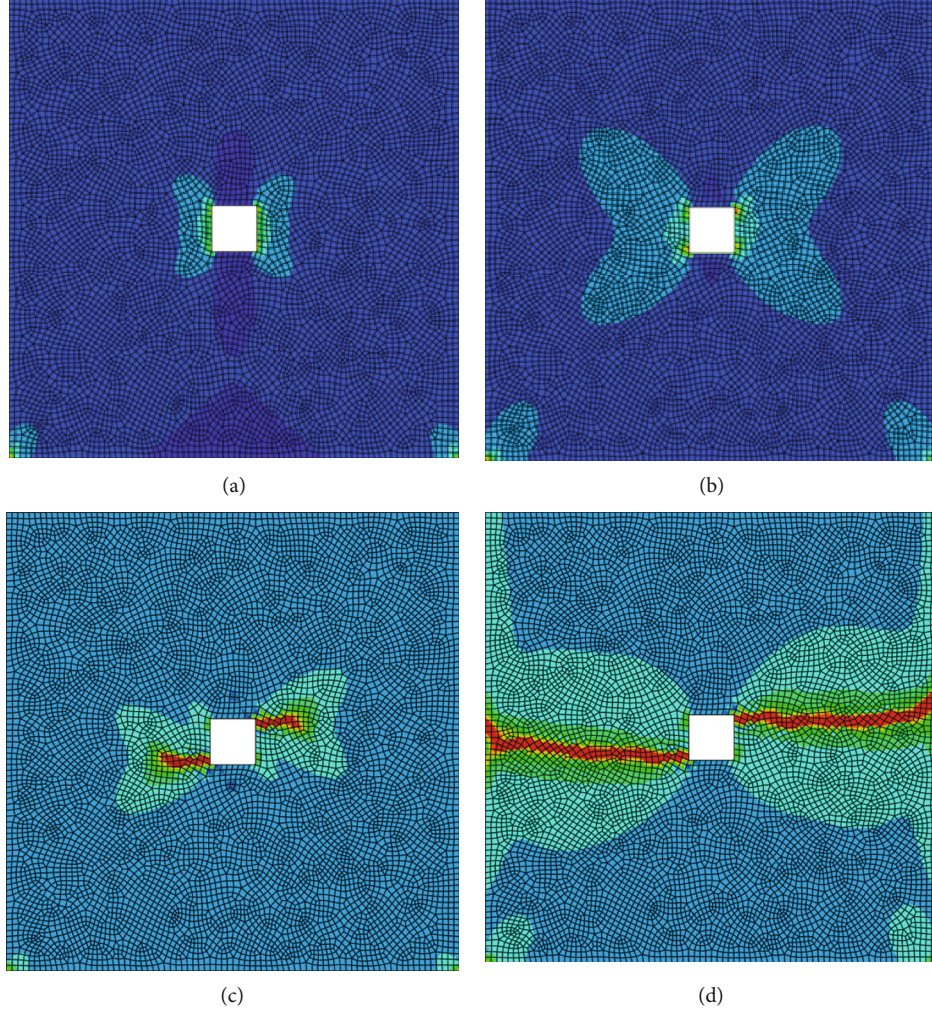
(a)

(b)

(c)

(d)

FIGURE 8: The result of crack propagation. (a) Crack initiation stage. (b) Crack initiation stage. (c) Crack development stage. (d) Crack penetration stage.

structure.

$$\partial W_{\text{int}} - \partial W_{\text{ext}} = 0. \qquad (12)$$

Combining Equations (8) with Equation (10), Dirichlet boundary conditions are considered, and Gauss theorem is used to obtain

$$\int_{\partial\Omega} [G_c l\nabla\phi \cdot \boldsymbol{n}] \cdot \delta\phi dA + \int_{\Omega}$$
$$\left\{ -[Div[\boldsymbol{\sigma}] + \boldsymbol{b}] \cdot \delta\boldsymbol{u} - \left[2(1-\phi)\psi(\varepsilon) - G_c \left[\frac{1}{l}\phi + Div(l\nabla\phi) \right] \right] \delta\phi \right\} dV$$
$$+ \int_{\partial\Omega_h} [\boldsymbol{\sigma} \cdot \boldsymbol{n} - \boldsymbol{h}] \cdot \delta\boldsymbol{u} dA = 0,$$

$$(13)$$

where n is the unit vector perpendicular to the plane.

Considering the Neumann boundary conditions $\boldsymbol{\sigma} \cdot \boldsymbol{n} = \boldsymbol{h}$ (on $\partial\Omega_h$) and $\nabla\phi \cdot \boldsymbol{n} = 0$ (on $\partial\Omega$), the strong form of the gov-

erning equation of the phase field method fracture model is

$$\begin{cases} Div[\boldsymbol{\sigma}] + \boldsymbol{b} = 0, \\ G_c \left[\frac{1}{l}\phi + l\nabla\phi \right] - 2(1-\phi)\psi(\varepsilon) = 0. \end{cases} \qquad (14)$$

3. Realize Fracture Finite Element by Using Phase Field Method

In order to solve the numerical solution of partial differential Equation (14), the weak form of the governing equation is solved by finite element method.

$$\begin{cases} \int_{\Omega} [\sigma\delta\varepsilon - \boldsymbol{b} \cdot \delta\boldsymbol{u}] \mathrm{d}V + \int_{\partial\Omega_h} h \cdot \delta\boldsymbol{u} dA = 0, \\ \int_{\Omega} \left\{ -2(1-\phi)\delta\phi\psi(\varepsilon) + G_c \left[\frac{1}{l}\phi\delta\phi + l\nabla\phi \cdot \nabla\delta\phi \right] \right\} dV = 0. \end{cases}$$

$$(15)$$

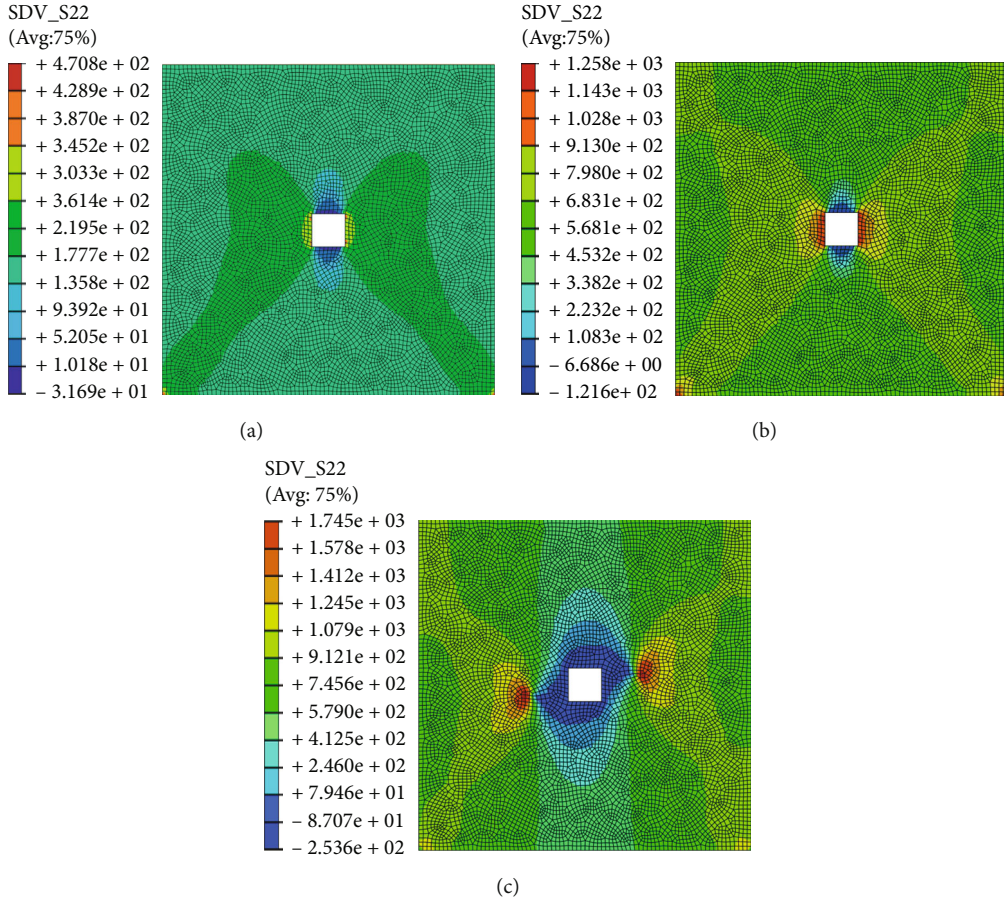Using the Voigt-notation method for discretization,

FIGURE 9: The vertical stress when the crack grows. (a) Crack initiation stage. (b) Crack initiation stage. (c) Crack development stage.

displacement field variables u and phase field variables ϕ on cell nodes I can be expressed as

$$\boldsymbol{u} = \sum_{i=1}^{n} N_i^u \boldsymbol{u}_i, \phi = \sum_{i=1}^{n} N_i^u \phi_i, \qquad (16)$$

where n is the number of nodes on a cell; N_i is the corresponding shape function on the node I, and the shape function matrix in two-dimensional case is

$$N_i^u = \begin{bmatrix} N_i & 0 \\ 0 & N_i \end{bmatrix}. \qquad (17)$$

Accordingly, the derivative of the form function can be discretized as

$$\boldsymbol{\varepsilon} = \sum_{i=1}^{n} \boldsymbol{B}_i^u \boldsymbol{u}_i, \nabla \phi = \sum_{i=1}^{n} \boldsymbol{B}_i^\phi \phi_i, \qquad (18)$$

where $\boldsymbol{\varepsilon} = [\varepsilon_{xx}, \varepsilon_{yy}, \varepsilon_{xy}]^T$.

Strain-displacement matrix and phase field matrix are

$$\boldsymbol{B}_i^u = \begin{bmatrix} N_{i,x} & 0 \\ 0 & N_{i,y} \\ N_{i,y} & N_{i,x} \end{bmatrix}, \boldsymbol{B}_i^\phi = \begin{bmatrix} N_{i,x} \\ N_{i,y} \end{bmatrix}. \qquad (19)$$

Then, the gradient of displacement variable and phase field variable can be expressed as

$$\delta \boldsymbol{\varepsilon} = \sum_{i=1}^{n} \boldsymbol{B}_i^{\delta u} \boldsymbol{u}_i, \nabla \phi = \sum_{i=1}^{n} \boldsymbol{B}_i^\phi \delta \phi_i. \qquad (20)$$

To ensure that $\partial W_{\text{int}} - \partial W_{\text{ext}} = 0$ for any u and ϕ, and, therefore, to ensure balance, the residual of its equation can be expressed as

$$R_i^u = \int_\Omega \left[(1-\phi)^2 + k\right] (\boldsymbol{B}_i^u)^T \sigma dV - \int_\Omega (N_i^u)^T b dV - \int_{\partial \Omega_h} (N_i^u)^T h dA,$$

$$R_i^\phi = \int_\Omega \left\{ -2(1-\phi)N_i \psi(\varepsilon) + G_c \left[\frac{1}{l} N_i \phi + l \left(\boldsymbol{B}_i^\phi \right)^T \nabla \phi \right] \right\} dV. \qquad (21)$$
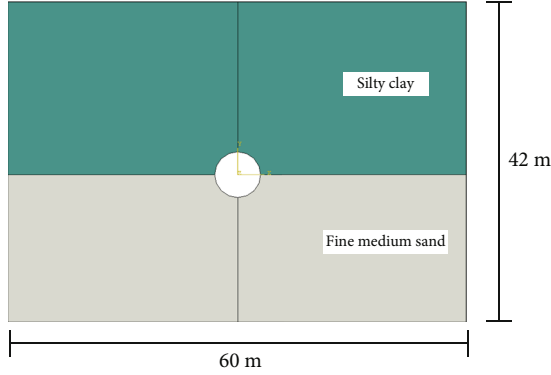
In order to get the residual close to 0, Newton-Raphson

FIGURE 10: Initial model around pile No. 21+979.

TABLE 1: Parameters of geological model around pile No. 21+979.

Number	Stratum	Density (10^3kg/m^3)	Elasticity modulus (MPa)	Poisson's ratio
1	Silty clay	1.96	5.94	0.3
2	Fine medium sand	2.00	13.5	0.2

method is used for incremental iteration.

$$\begin{Bmatrix} u \\ \phi \end{Bmatrix}_{t+\Delta t} = \begin{Bmatrix} u \\ \phi \end{Bmatrix}_t - \begin{bmatrix} K^{uu} & K^{u\phi} \\ K^{\phi u} & K^{\phi\phi} \end{bmatrix}_t^{-1} \begin{Bmatrix} R^u \\ R^\phi \end{Bmatrix}_t. \tag{22}$$

The governing equation is a partial differential equation system composed of quasi-static equilibrium equation and phase field equation. However, in order to prevent crack closure when the elastic body is under pressure or unloading springback and ensure the irreversible process of crack evolution ($\phi_{t+\Delta t} \geq \phi_t$), a historical state variable H is introduced to realize the irreversible process.

$$H = \begin{cases} \psi(\varepsilon), \psi(\varepsilon) > H_t \\ H_t, \psi(\varepsilon) \leq H_t \end{cases}. \tag{23}$$

Therefore, after considering the historical state variables, the residual corresponding to phase field crack evolution is

$$R_i^\phi = \int_\Omega \left\{ -2(1-\phi)N_i H + G_c \left[\frac{1}{l} N_i \phi + l \left(\mathbf{B}_i^\phi \right)^T \nabla\phi \right] \right\} dV. \tag{24}$$

The residual of the displacement field is

$$R_i^u = \int_\Omega \left[(1-\phi)^2 + k \right] (\mathbf{B}_i^u)^T \sigma dV - \int_\Omega (N_i^u)^T b dV - \int_{\partial\Omega_h} (N_i^u)^T h dA. \tag{25}$$

The stiffness matrix gradually degenerates in the process of crack initiation and propagation, which will result in constant rearrangement of the stress field. The implicit solver
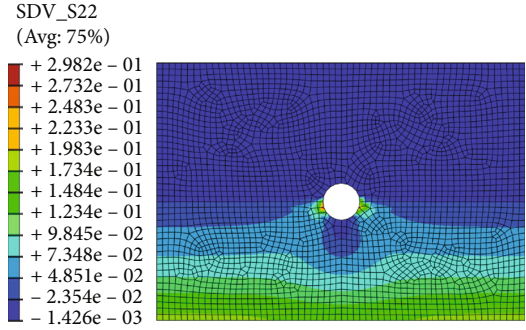

FIGURE 11: Crack propagation under the disturbance of excavation.

cannot be used to obtain a stable equilibrium solution. Therefore, the displacement field and phase field in Equation (14) are considered as coupling fields and solved separately. Considering the historical state variables, Equation (14) can be expressed as

$$G_c \left[\frac{1}{l} \phi + l\nabla\phi \right] - 2(1-\phi)H = 0. \tag{26}$$

By using the Newton-Raphson method for iteration, the Equation (23) can be expressed as

$$\begin{Bmatrix} u \\ \phi \end{Bmatrix}_{t+\Delta t} = \begin{Bmatrix} u \\ \phi \end{Bmatrix}_t - \begin{bmatrix} K^{uu} & 0 \\ 0 & K^{\phi\phi} \end{bmatrix}_t^{-1} \begin{Bmatrix} R^u \\ R^\phi \end{Bmatrix}_t, \tag{27}$$

where each stiffness matrix is

$$\begin{cases} K_{ij}^{uu} = \dfrac{\partial R_i^u}{\partial u_j} = \int_\Omega \left[(1-\phi)^2 + k \right] (\mathbf{B}_i^u)^T \mathbf{C}_0 \mathbf{B}_j^u dV, \\ K_{ij}^{\phi\phi} = \dfrac{\partial R_i^\phi}{\partial \phi_j} = \int_\Omega \left\{ \left[2H + \dfrac{G_c}{l} \right] N_i N_j + G_c l \left(\mathbf{B}_i^\phi \right)^T \mathbf{B}_j^\phi \right\} dV. \end{cases} \tag{28}$$

In this paper, ABAQUS is used to realize the phase field method fracture simulation. This research realized the phase field method model by using UEL of ABAQUS. The relevant stiffness matrix is updated in UEL. The specific process is shown in Figure 2. Due to the use of user element subroutine, the integral points defined by it cannot be visualized independently in ABAQUS postprocessing. However, the element stiffness matrix and stress-strain results on each node can be obtained. In order to realize the visualization of the results, this paper creates an auxiliary grid by using UMAT to define the relevant material parameters at each integral point of the auxiliary grid. Then, transmit the data of user unit subroutine to user material subroutine, and output SDV variables for final visualization. The stress component and stiffness matrix of the auxiliary virtual grid are zero, which have no influence on the solution result.
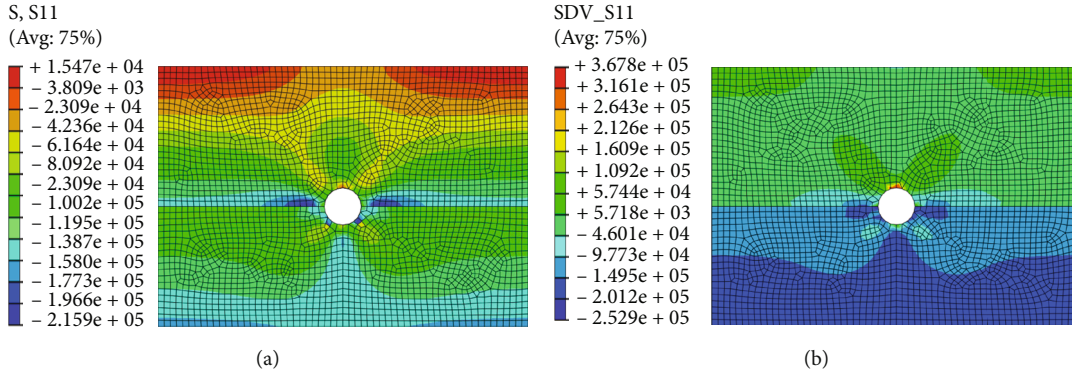
FIGURE 12: Horizontal stress distribution after excavation. (a) No cracks. (b) Consider cracks.
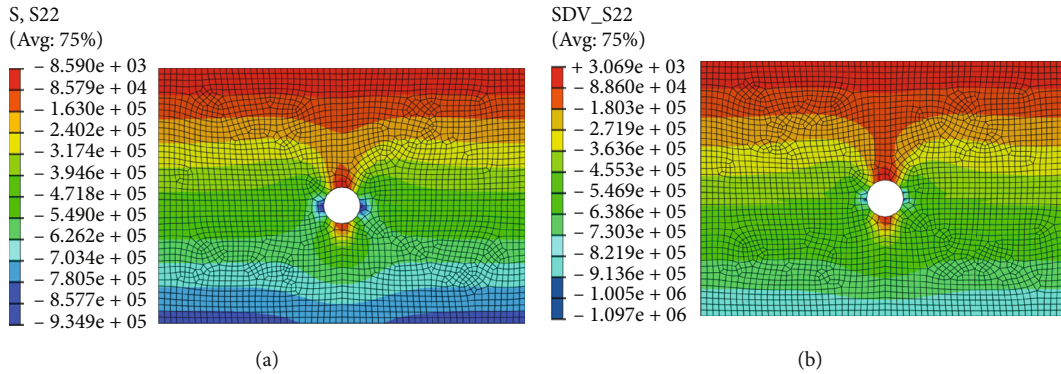

FIGURE 13: Vertical stress distribution after excavation. (a) No cracks. (b) Consider cracks.

4. Numerical Simulation Examples and Verification

4.1. A Case of Prefabricated Crack Propagation. To verify the correctness of the code, a square plate with prefabricated cracks on the left side was created. The specific size of the plate is shown in Figure 3. The lower boundary of the model was fixed. The upward displacement plate of 0.01 mm was applied to the upper boundary. The Young's modulus $E = 210 GPa$. Poisson's ratio is $\mu = 0.3$. The critical energy release rate is $G_c = 2.7 \times 10^{-3} kN/mm$.

In this paper, the crack length parameters were, respectively, selected as $l = 0.015$mm and $l = 0.0075$mm. The crack propagation results are shown in Figures 4 and 5. In the figure, the blue area represented no failure, while the red area represented complete failure. The fracture initiates in a butterfly shape and then expands along the horizontal and vertical direction. Finally, the crack reaches the right side of the model.

Figure 6 shows the comparison between the reaction force and displacement curve calculated in this paper and Miehe [27]. At that time, the maximum support reaction force calculated was 0.71 kN, and the maximum support reaction force calculated was 0.74 kN. The calculation results were basically consistent with the crack growth and support reaction displacement curve obtained by Miehe. Although there is a small deviation on the curve, the maximum reaction force is basically similar, which is consistent with the results of Miehe. It is found that with the increase of l, while

the maximum reaction force decreases. The result verifies the correctness of the phase field code.

4.2. A Case of Tensile Crack Propagation of Perforated Plate. A square plate with side length of 40 m was established. And a square hole with one side length of 4 m was established in the center of the plate, as shown in Figure 7. Young's modulus $E = 210 GPa$, Poisson's ratio $\mu = 0.3$, and critical energy release rate $G_c = 2.7 \times 10^{-3} kN/mm$ were used to fix the lower boundary of the CPE4 unit model, and upward displacement was applied to the upper boundary of the model. The lower boundary of the CPE4 element model is fixed, and the upper boundary of the model is subjected to upward displacement.

Characteristic length $l = 0.04$m. The crack extension results are shown in Figure 8. The results showed that symmetrical butterfly-shaped microcracks appear around the hole in the initial stage. At this time, the structure damage was small. As the tension continued to be applied, the butterfly area expanded, eventually creating cracks in the upper right and lower left corners of the square hole. And the crack continued to expand and develops to the edge of the model, which proved the feasibility of crack initiation and self-propagation.

The variation of vertical stress with crack growth in this example is shown in Figure 9. The results showed that there was a great stress concentration at the four corners of the hole at the initial stage of crack development. And the stress distribution likes the butterfly. The maximum vertical stress was 4.7×10^2 MPa. The stress on both sides of the hole
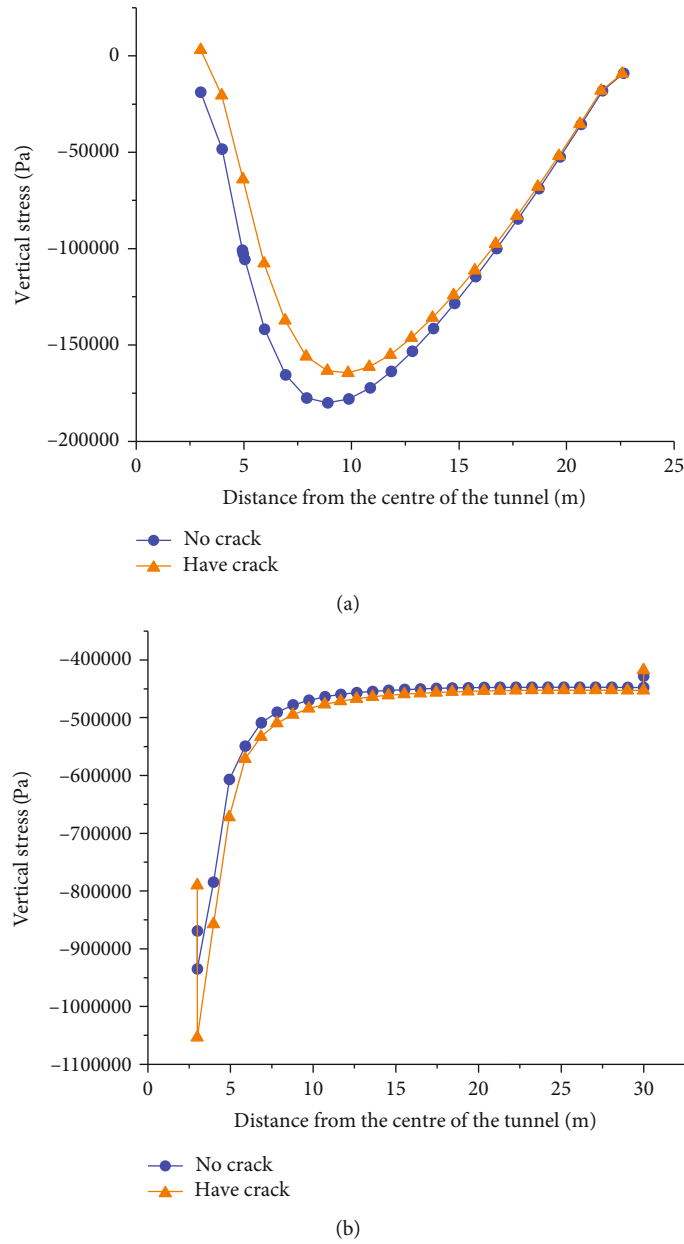
(a)

(b)

FIGURE 14: Comparison of vertical stress after excavation. (a) Above the vertical axis of the tunnel. (b) Right of horizontal axis of tunnel.

gradually increased and gradually formed a butterfly region until the fracture occurs. The stress on both sides of the hole is positive, and the stress above and below the hole is negative. The maximum vertical stress was 1.23×10^3 MPa. Crack propagation begins at this time. After that, the crack propagated gradually. And the butterfly stress distribution was still present at the end of crack propagation. At this time, the maximum vertical stress was 1.7×10^3 MPa.

4.3. A Case of Crack Propagation in Composite Stratum Disturbed by Excavation

4.3.1. Engineering Background. As a strategic project in China, the South-to-North Water Diversion Project is an

extremely large infrastructure project to solve the serious shortage of water resources in the north and implement the optimal allocation of water resources. It plays a very important role in alleviating the bearing pressure of water resources and improving the water supply security and guarantee rate in Beijing.

Under the influence of excavation disturbance, some stress concentration occurs in the geological body of Eastern Canal in Beijing, which leads to lining damage and pipeline leakage. Therefore, the pile no. 21+979 and its surrounding area of Eastern Canal of the South-to-North Water Diversion Project were selected for the analysis. Crack propagation and stress disturbance were analyzed in this case. The left and right width of the numerical model near pile no.
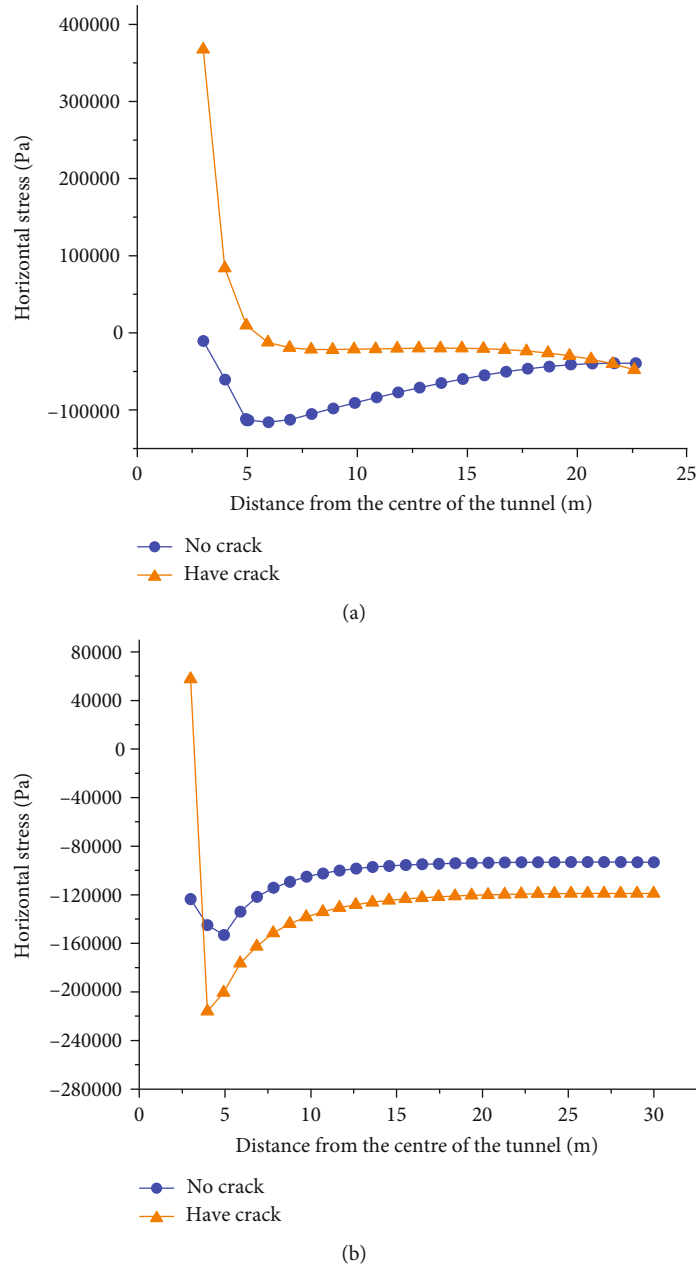
(a)

(b)

FIGURE 15: Comparison of horizontal stress after excavation. (a) Above the vertical axis of the tunnel. (b) Right of horizontal axis of tunnel.

21+979 is 60 m. The tunnel buried depth is 19.62 m. The depth below the axis of the tunnel is 22.38 m and the tunnel radius is 3 m.

According to the site geological survey data, the strata were simplified, and a composite stratum tunnel model was established. The tunnel size and stratum distribution are shown in Figure 10. The material parameters are shown in Table 1. Material critical energy release rate is $G_c = 2.7 \times 10^{-3} kN/mm$. Controlling the parameters of diffuse crack width is $l = 0.04$m.

4.3.2. Realization of Phase Field Method. In order to simulate the initial stress state of rock and soil mass, the ground stress balance was carried out first. Then, the excavation was car-

ried out. The specific process of the excavation of rock and soil mass simulated based on the phase field method is as follows:

(1) Establish the initial composite formation model (without tunnel excavation). Fix the bottom boundary for the model, $u_x = 0$ and $u_y = 0$. The left and right boundaries of the model are fixed with normal displacement, $u_x = 0$. The initial geostress field of the model was obtained by the ground stress balance analysis step under the dead weight stress

(2) Delete some excavated units, renumber nodes and grids, and establish tunnel excavation model

(3) In the .inp file of ABAQUS, the fracture parameters related to the layer phase field method were defined and the virtual visualization grid was generated. Apply the initial in situ stress field calculated in the first step to the tunnel excavation model, and define the output variables to simulate the excavation of rock and soil mass, which considered the phase field method

Considering the crack growth, the crack growth is shown in Figure 11. After tunnel excavation, the cracks of the model are mainly distributed around the tunnel, and the weak links are on the horizontal sides of the tunnel. The crack initiation occurs firstly in horizontal direction and then gradually develops. After excavation, the stress of the tunnel is released, and the shape of tunnel is ellipse. Due to the maximum stress on both sides of the middle line of the tunnel, there is a large damage in this part. The crack begins to expand at the horizontal direction.

The horizontal stress cloud diagram after excavation is shown in Figure 12. Figure 12(a) is the horizontal stress result obtained without considering the phase field method, that is, without crack development; Figure 12(b) is the horizontal stress result obtained with crack development by using the phase field method. Both cases indicate that stress disturbance occurs in the surrounding area after tunnel excavation. When the crack is not considered, the maximum horizontal stress is 2.16×10^5 Pa, which occurs near the horizontal axis of the tunnel waist. When considering the crack, the maximum stress on the horizontal axis is 2.53×10^5 Pa, and it is found that the stress at the tunnel dome increases significantly, up to 3.68×10^5 Pa. It indicates that the crack development has a great influence on the stress.

The vertical stress cloud is shown in Figure 13. In situ stress is disturbed after excavation. When do not consider the crack, the maximum stress can reach 9.35×10^5 Pa. It occurs at the horizontal axis of the tunnel edge. When considering the crack development, the stress level around the tunnel increases due to the influence of the crack development. The maximum stress can reach 1.10×10^6 Pa. At the horizontal axis of the tunnel edge, the stress at the dome changes under the influence of the crack. It produces a vertical upward stress of 3.07×10^3 Pa.

After the phase field method is adopted to simulate the excavation, the stress around the tunnel changes greatly from considering the cracks, which is due to the development of cracks around the tunnel. In the area far away from the tunnel, it is less affected by the crack, as shown in Figures 14 and 15. However, its total stress level is reduced, which is due to part of the elastic energy into the surface energy of the crack. As the cracks developed along the horizontal axis, it can be found in Figure 14(b) and Figure 15(b) that when the distance from the center of the tunnel is 3 m (tunnel boundary), the stress level of the cracks is significantly different from that when the crack is not considered. The vertical stress reaches -7.90×10^5 MPa when the crack is considered. The vertical stress reaches -8.69×10^5 MPa when the crack is not considered. The horizontal stress is 5.76×10^4 MPa when the crack is considered and -1.24×10^5 MPa when the crack is not considered.

5. Conclusion

Based on ABAQUS platform, this paper realized the phase field method fracture model and simulated the crack growth of composite stratum under excavation disturbance. This paper realized the excavation simulation of composite stratum based on the phase field method. The main conclusions are as follows:

(1) By using UMAT/UEL of ABAQUS secondary development interface, prefabricated crack growth simulation, prefabricated hole crack growth simulation, and composite stratum crack growth simulation under excavation disturbance were carried out. Based on the previous phase field model, the simulation of various materials and the disturbance analysis of excavation to the model are realized in this paper

(2) The correctness and reliability of the phase field fracture model code were verified by comparing the results of prefabricated crack propagation simulation with those in other literature. It was found that the crack propagated in the upper right corner and the lower left corner of the hole through the tensile example of the perforated plate, which demonstrated the feasibility of the phase field method for the self-initiation and propagation of cracks. By comparing the crack growth model under excavation disturbance with the model without crack growth, it was found that the stress disturbance was great at the crack development. When considering the crack, the maximum stress on the horizontal axis was 2.53×10^5 Pa. It was found that the stress at the tunnel dome increased greatly, up to 3.68×10^5 Pa

(3) Based on the crack propagation model of composite strata established by phase field method, the crack distribution of rock mass after excavation disturbance and the fine in situ stress distribution around the tunnel are obtained. It provides an idea for simulating crack propagation in geotechnical engineering and lays a foundation for simulating in situ stress analysis in geotechnical excavation engineering

Data Availability

The data used to support the findings of this study are included within the article.

Conflicts of Interest

There is no conflict of interest regarding the publication of this paper.

Acknowledgments

References

[1] H. Lin, H. Yang, Y. Wang, Y. Zhao, and R. Cao, "Determination of the stress field and crack initiation angle of an open flaw tip under uniaxial compression," *Theoretical and Applied Fracture Mechanics*, vol. 104, p. 102358, 2019.

[2] H. Yang, H. Lin, Y. Chen et al., "Influence of wing crack propagation on the failure process and strength of fractured specimens," *Bulletin of Engineering Geology and the Environment*, vol. 81, no. 1, 2022.

[3] R. Fan and J. Fish, "Thers-method for material failure simulations," *International Journal for Numerical Methods in Engineering*, vol. 73, no. 11, pp. 1607–1623, 2008.

[4] J. Hallquist, *LS-DYNA Theoretical Manual*, Livemore Software Technology Corporation, USA, 1998.

[5] X. P. Xu and A. Needlemana, "*Numerical simulation of fast crack growth in brittle solids*," *Journal of the Mechanics and Physics of Solids*, vol. 9, no. 42, pp. 1397–1434, 1994.

[6] G. Tcamacho and M. Ortiz, "Computational modelling of impact damage in brittle materials," *International Journal of Solids and Structures*, vol. 33, no. 20-22, pp. 2899–2938, 1996.

[7] C. H. Sam, D. Katerina, and A. Stephen, "Obtaining initially rigid cohesive finite element models that are temporally convergent," *Engineering Fracture Mechanics*, vol. 72, no. 14, pp. 2247–2267, 2005.

[8] L. B. Lucy, "A numerical approach to the testing of the fission hypothesis," *The Astronomical Journal*, vol. 82, pp. 1013–1013, 1977.

[9] R. A. Gingold and J. J. Monaghan, "Smoothed particle hydrodynamics: theory and application to non-spherical stars," *Monthly Notices of the Royal Astronomical Society*, vol. 181, no. 3, pp. 375–389, 1977.

[10] B. Nayroles, G. Touzot, and P. Villon, "Generalizing the finite element method: diffuse approximation and diffuse elements," *Computational Mechanics*, vol. 10, no. 5, pp. 307–318, 1992.

[11] T. Belytschko and T. Black, "Elastic crack growth in finite elements with minimal remeshing," *International Journal for Numerical Methods in Engineering*, vol. 45, no. 5, pp. 601–620, 1999.

[12] M. Nicolas, D. John, and B. Ted, "A finite element method for crack growth without remeshing," *International Journal for Numerical Methods in Engineering*, vol. 46, no. 1, pp. 131–150, 1999.

[13] B. Ted, C. Hao, X. Jingxiao, and Z. Goangseup, "Dynamic crack propagation based on loss of hyperbolicity and a new discontinuous enrichment," *International Journal for Numerical Methods in Engineering*, vol. 58, no. 12, pp. 1873–1905, 2003.

[14] J. H. Song, P. Areias, and B. Ted, "A method for dynamic crack and shear band propagation with phantom nodes," *International Journal for Numerical Methods in Engineering*, vol. 67, no. 6, pp. 868–893, 2006.

[15] H. Vincent and K. Alain, "Laws of crack motion and phase-field models of fracture," *Journal of the Mechanics and Physics of Solids*, vol. 57, no. 2, 2009.

[16] H. Zhang, J. D. Yu, and X. Y. Pei, "Development of phase field fracture methods," *Chinese Journal of High Pressure Physics*, vol. 33, no. 3, pp. 128–139, 2019.

[17] M. P. Emilio, G. Alireza, and F. Christian, "A phase field formulation for hydrogen assisted cracking," *Computer Methods in Applied Mechanics and Engineering*, vol. 342, pp. 742–761, 2018.

[18] M. Christian and L. M. Schänzel, "Phase field modeling of fracture in rubbery polymers. Part I: Finite elasticity coupled with brittle failure," *Journal of the Mechanics and Physics of Solids*, vol. 65, pp. 93–113, 2014.

[19] M. Hofacker and C. Miehe, "A phase field model of dynamic fracture: robust field updates for the analysis of complex crack patterns," *International Journal for Numerical Methods in Engineering*, vol. 93, no. 3, 2013.

[20] K. Park, G. Paulino, W. Celes, and R. Espinha, "Adaptive mesh refinement and coarsening for cohesive zone modeling of dynamic fracture," *International Journal for Numerical Methods in Engineering*, vol. 92, no. 1, 2012.

[21] G. W. Liu, Q. B. Li, and Z. Zuo, "Implementation of phase field fracture model step algorithm in ABAQUS," *Chinese Journal of Rock Mechanics and Engineering*, vol. 35, no. 5, pp. 1019–1030, 2016.

[22] Y. K. Cao, K. K. Sun, and S. X. Zhu, "Elastoplastic fracture simulation of a plate with holes based on phase field method," *Ordnance Materials Science and Engineering*, vol. 44, no. 2, pp. 39–44, 2021.

[23] J. Liu, Y. Xue, and F. Gao, "Study on hydraulic fracture propagation of layered shale by phase field method," *Chinese Journal of Geotechnical Engineering*, vol. 44, no. 3, pp. 1–9, 2021.

[24] A. Griffith, "The phenomena of rupture and flow in solids," *Physical and Engineering Sciences*, vol. 221, no. 582-593, pp. 163–198, 1921.

[25] G. Afrancfort and J. Jmarigo, "Revisiting brittle fracture as an energy minimization problem," *Journal of the Mechanics and Physics of Solids*, vol. 46, no. 8, pp. 1319–1342, 1998.

[26] Bourdin, *The Variational Approach to Fracture*, Springer, 2008.

[27] C. Miehe, F. Welschinger, and M. Hofacker, "Thermodynamically consistent phase-field models of fracture: variational principles and multi-field FE implementations," *International Journal for Numerical Methods in Engineering*, vol. 83, no. 10, pp. 1273–1311, 2010.